Surface & Coatings Technology 359 (2019) 62–72

Contents lists available at ScienceDirect

Surface & Coatings Technology

journal homepage: www.elsevier.com/locate/surfcoat

Roughening of hollow glass microspheres by NaF for Ni electroless plating

Jianfeng Zhang[a,*], Xuepan Yang[a], Songbai Yu[a], Mengni Ge[a], Fanxu Meng[a], Jun Wang[b], Xiyuan Wu[b], Wan Jiang[c]

[a] College of Mechanics and Materials, Hohai University, Nanjing 211100, China
[b] Sinosteel Maanshan New Material Technology Co., Ltd, Maanshan 243000, China
[c] College of Materials Science and Engineering, Donghua University, Shanghai 201620, China

ARTICLE INFO

Keywords:
Electroless chemical plating
Hollow glass microspheres (HGMs)
NaF roughening
Mechanism

ABSTRACT

Roughening of non-conductive substrate ceramic materials with hydrofluoric acid (HF) is usually an essential step to enhance adhesion of the coating by electroless chemical plating. However, the violent reaction between HF and the hollow glass microspheres (HGMs) usually causes breakage and damage of the thin shells of HGMs. This paper proposes a modified roughening strategy for Ni electroless plating, i.e., eroding HGMS slowly with a mixture of sodium fluoride (NaF) and hydrochloric acid (HCl). The Na_2SiF_6 by-products from the reaction of NaF with SiO_2 were erased by the following NaOH washing to expose the surface of HGMs without any obvious pores or breakage. Such a modified roughening and followed alkali washing strategy can thus not only reduce the surface corrosion, but also hinder the further damage of HGMs by covering Na_2SiF_6 sediments. The successive plating of uniform Ni nanoparticles on HGMs was conducted, and the related mechanism was discussed in detail.

1. Introduction

Hollow glass microspheres (HGMs), mainly made of fly ash with main components of silica, are now attracting more and more attention due to the merits of high compressive strength, high fire resistance, high corrosion resistance, low thermal conductivity and low thermal shrinkage coefficient. They can be used for petroleum drilling [1], composite material [2,3], hydrogen storage [4], drug diagnosis [5] and so on. Simultaneously, the further surface metallization of HGMs by cobalt [6–8], nickel-cobalt [9], nickel-iron [10,11] and iron-cobalt [12], would like render them as ultra-light multifunctional materials for conduction fillers and wave absorbents.

Many methods, such as chemical vapor deposition [13,14], sol-gel method [15], sputtering deposition [16] and electroless chemical plating [17–19] have been used for surface metallization of HGMs. Among them, electroless chemical plating is one of the most often used with the advantages of simplicity and easy operation. It is usually composed of the following steps, (i) surface roughening, (ii) surface activation and (iii) chemical plating. Among these steps, activation has been paid much attention to make the substrate surface covered with a layer of metal for self-catalytic ability. Just because of this reason, most literatures are dealing with the optimization of such step or developing non-noble metals for activation. For example, Shukla et al. coated copper on HGMs using a $AgNO_3$ activator instead of the traditional $PdCl_2$ activator [20]. Meng et al. prepared magnetic HGMs composite material by activating electroless Ni plating using Ni salt [21]. Zhang et al. activated the surface of ABS plastics by novel palladium-free pretreatments by molecular grafting and self-assembling for Ni plating [22].

However, roughening is also of vital importance to increase the micro-roughness and contact area of the substrate surface, and then to improve the adhesion and wettability between the substrate and the coating [23]. Therefore, this step determines the uniformity of the coating and the adhesion strength between the coating and the substrate directly [24]. HF is mostly often used as the roughening agent for commercial HGMs as silica is inert to most other common acids. But the strong exothermic reaction of SiO_2 with HF would like to cause the breakage of the thin wall of HGMs, and then low quality, i.e., discontinuous and even easy-to-fall-off plating. Some material scientists have also tried to pre-treat the surface of HGMs by NaOH hydroxylating [25], potassiu mdichromate ($K_2Cr_2O_7$) plus sulfur acid (H_2SO_4, 98 wt%) [6], or γ-aminopropyltriethoxy silane (APS) [10]. But the weak adhesion between the plating layer and the smooth substrate surface of HGMs is still a problem should be conquered urgently.

Compared with other metal deposition on HGMs, such as Cu [26] and Ag [27], Ni plating is also much more important due to its outstanding corrosion and wear resistance [28]. In addition, Ni plating is also used to make a soft magnetic thin film with excellent high

* Corresponding author.
E-mail address: jfzhang@hhu.edu.cn (J. Zhang).

https://doi.org/10.1016/j.surfcoat.2018.12.031
Received 6 September 2018; Received in revised form 6 December 2018; Accepted 7 December 2018
Available online 08 December 2018
0257-8972/

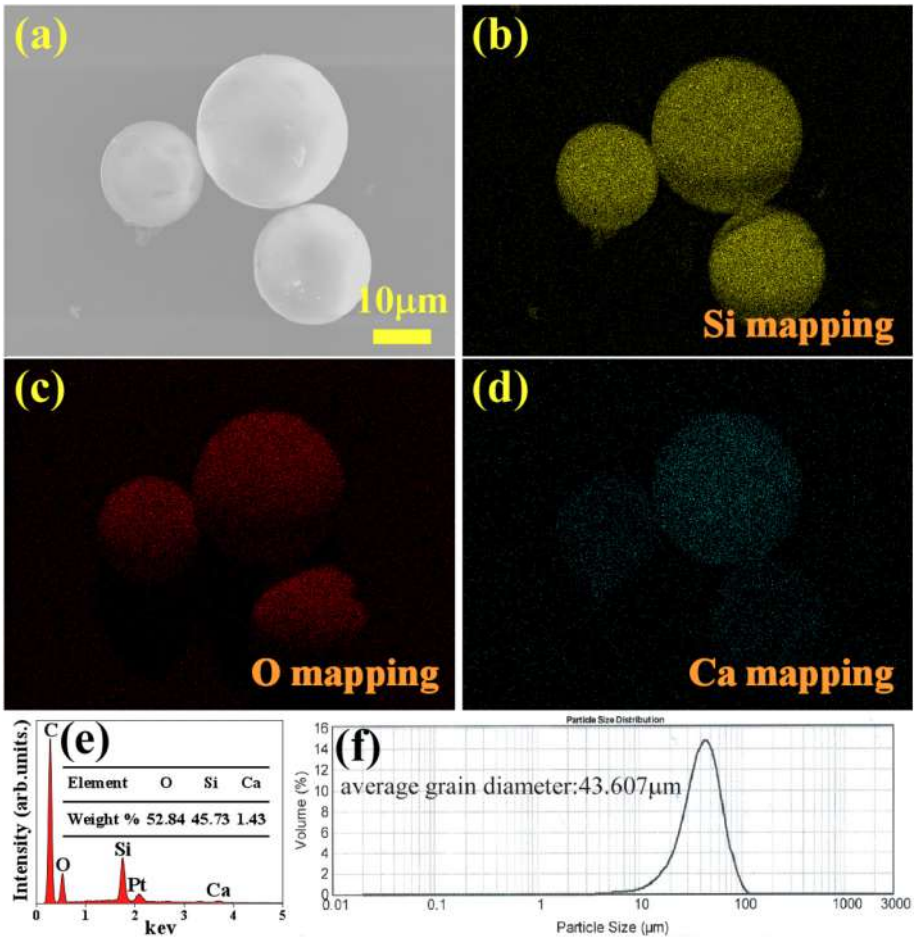

Fig. 1. Characterization of pristine HGMs. (a) SEM image, (b) Si mapping, (c) O mapping, (d) Ca mapping, (e) EDX spectrum and (f) size distribution.

frequency electromagnetic properties [21]. This paper proposes a new and feasible NaF roughening method for Ni plating, i.e., pre-treating HGMs by soaking in a mixed solution of NaF with HCl. The following activation by $PdCl_2$ and final Ni plating indicated that uniform Ni nanoparticles were uniformly dispersed on the surface of HGMs. The effects of NaF and NaOH concentration on the recovery ratio of HGMs were investigated, and the related mechanism was discussed in comparison with HF roughening.

2. Experimental procedure

2.1. Raw materials

As shown in Fig. 1, HGMs supplied by Sinosteel Maanshan Institute of Mining Research Co., Ltd., were 5–100 μm in diameter and 0.6 g cm^{-3} in true density. The main element of HGMs are Si and O and also contains a small amount of Ca. The analytical reagents, including sulfate hexahydrate ($NiSO_4{\cdot}6H_2O$), Sodium hypophosphite monohydrate ($NaH_2PO_2{\cdot}H_2O$), trisodium citrate dehydrate ($C_6H_5Na_3O_7{\cdot}2H_2O$) and sodium acetate trihydrate ($CH_3COONa{\cdot}3H_2O$), were purchased from Sinopharm Chemical Reagent Co., Ltd., and used as received without any further treatment.

2.2. Electroless Ni plating process

Fig. 2 shows the experimental strategy, including roughening, activation and then Ni plating, as described in brief as follows.

a) Roughening of HGMs were conducted by soaking two different solutions separately: (a_1) in HF solution (0.5–4.5 mol/L, 0.1 L) for 30 s, followed by drying at 60 °C for 1 h; (a_2) in a mixed NaF (0.5–4.5 mol/L) and HCl (2.5 mol/L) solution, followed by NaOH washing (0.1 L; 2.5 mol/L) for 30 min and drying at 60 °C for 1 h. The as-roughened HGMs were dispersed in deionized water and poured into a separator funnel to rest for 30 min. Then the broken HGMs were removed out due to the higher density (2.2 g·cm^{-3}) than water, which will be weighted afterwards.
b) Activation treatment of the HGMs after the former step was carried out in a colloid-palladium solution at 55 °C for 30 min, in which palladium chloride was set at 0.1 g/L. Then the activating HGMs were filtered from the solution, immersed in 10 vol% HCl for 2 min and later rinsed with distilled water for 3 min.
c) Ni plating on HGMs after the roughening and activation steps was carried out in a bath containing a mixture as shown in Table 1 for 30 min. The plating temperature and pH value of the bath was set at 75 °C and 4.8–5, separately. Both solution (0.1 L) and 1 g of activated microspheres were used as substrates. Mechanical agitation at a high rotation rate given to the electrolyte will damage the HGMs as well. After measuring the damage ratio of the filtrated microspheres, a uniform rotation rate (400 r/min) was employed in the full process to avoid the HGMs breakage caused by mechanical agitation as possible
d) Finally, the plated HGMs were filtered and dried at 60 °C before use.

2.3. Calculation

In order to determine the recovery ratio and broken ratio of the HGMs, the as-roughened HGMs were dried and weighted. The recovery

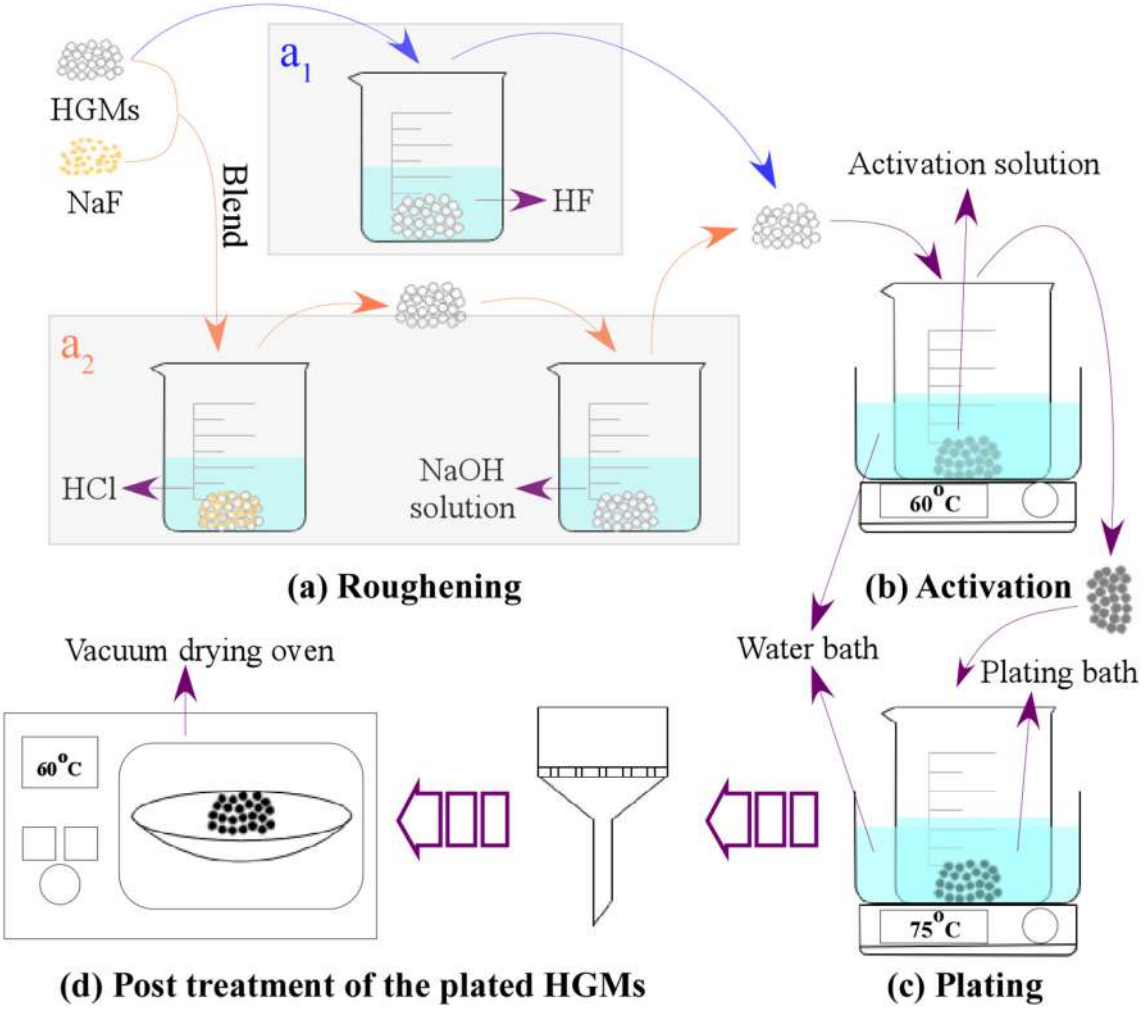

Fig. 2. Experimental flow chart for the modified roughening and electroless plating strategy.

Table 1
Composition and condition of plating bath.

Chemical	Concentration	Operation conditions
$NiSO_4$ $6H_2O$	25 g/L	Temperature: 75 °C,
NaH_2PO_2 H_2O	25 g/L	Stirring speed: 400 r/min
$C_6H_5Na_3O_7$ $2H_2O$	25 g/L	pH value: 4.8–5
CH_3COONa $3H_2O$	15 g/L	
Lactic acid	25 g/L	

ratio of HGMs in the process of roughening was set as r_1:

$$r_1 \frac{m_1}{m_0} \tag{1}$$

where m_0 represents the weight of raw HGMs, and m_1 represents the weight of roughened HGMs.

The broken ratio of roughening HGMs was set as r_2:

$$r_2 = \frac{m_2}{m_1} \tag{2}$$

where m_2 represents the weight of the broken HGMs, and m_1 represents the same weight of roughened HGMs in Eq. (1).

The roughened HGMs by NaF were immersed in boiling water in order to determine the proportion of NaF contributed to the generation SiF_4 or Na_2SiF_6, since the latter reacts with hot water to form HF according to the following reaction:

$$Na_2SiF_6 + 2H_2O \overset{Boiling}{\rightarrow} 2NaF + 4HF + Sio_2 \tag{3}$$

The acid-alkali titration method was used to determine the HF content as well as Na_2SiF_6 content. As the NaOH molar amount consumed in titration was set as n_0, the molar amount of Na_2SiF_6 (set as n) produced in the acid roughening reaction can be calculated according to the following reaction formula.

$$n = \frac{n_0}{4} \tag{4}$$

2.4. Characterization

The phase identification of the as-obtained microspheres was performed via X-ray diffraction (XRD, Bruker D8 VENTURE, Germany) with a Cu Kα radiation (λ = 1.5405 Å) powered at 40 kV/100 mA. The testing was carried out for 2θ scanning from 10° to 90° at a rate of 10°/min with a goniometric resolution of 0.02°. The surface morphology and microstructural features of composite microspheres were observed by field emission scanning electron microscopy (FESEM, SUPRA 55 SAPPHIRE, ZEISS, Germany) equipped with energy-dispersive X-ray spectroscopy (EDS, Oxford Inca Energy 400, U.K.).

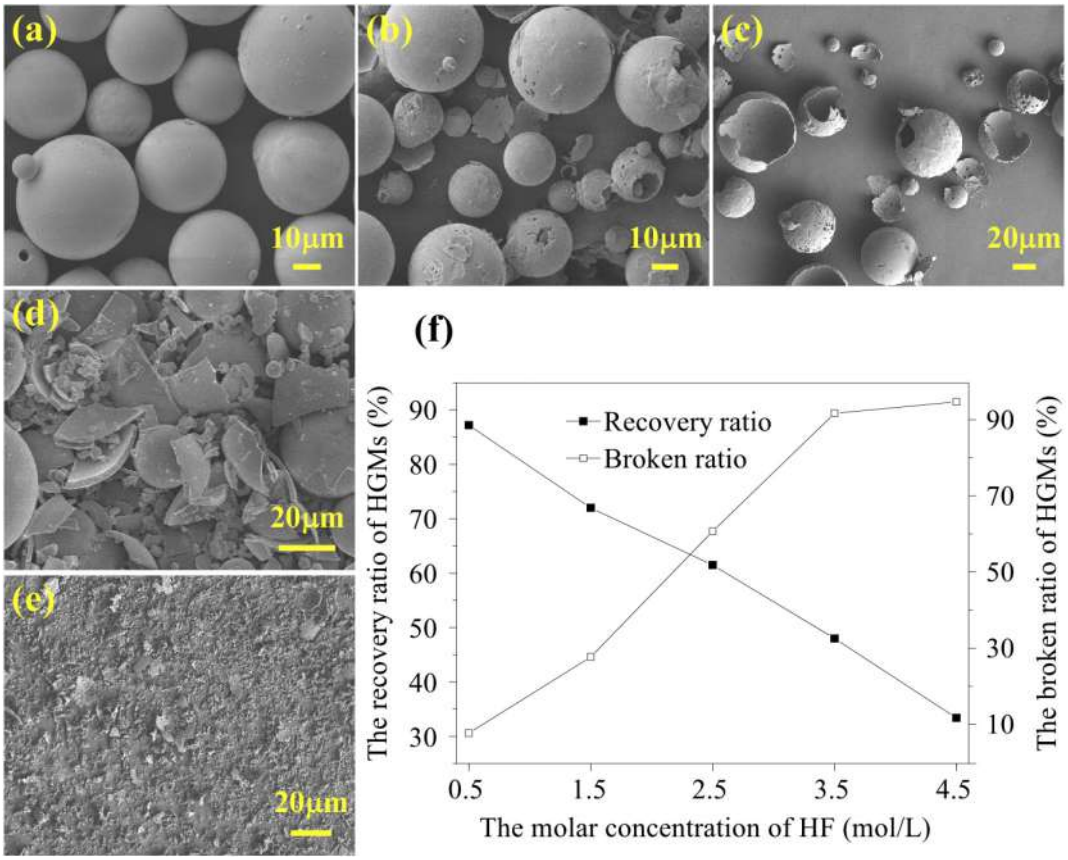

Fig. 3. SEM images of HGMs roughened with different concentrations of HF at (a) 0.5 mol/L, (b) 1.5 mol/L, (c) 2.5 mol/L, (d) 3.5 mol/L, (e) 4.5 mol/L and (f) the recovery ratio and broken ratio of HGMs roughened with different concentrations of HF.

3. Results and discussion

3.1. HF roughening

Fig. 3 shows the SEM images of HGMs roughened with different concentrations of HF at (a) 0.5 mol/L, (b) 1.5 mol/L, (c) 2.5 mol/L, (d) 3.5 mol/L, (e) 4.5 mol/L and (f) the dependence of recovery ratio/broken ratio on HF concentrations. At a low HF concentration of 0.5 mol/L, the recovery ratio of microspheres is as high as almost 87.3%, and the broken ratio is only about 10%, with a preferred integrity (Fig. 3(a)). With increasing the HF concentration to 1.5 mol/L and 2.5 mol/L, the recovery ratio of the microspheres decreases linearly and the broken ratio increases rapidly, reaching 28% and 61%, respectively. With the rising of the HF concentration further (3.5 mol/L and 4.5 mol/L), the broken ratio reached close to 90%, and only very few complete HGMs were observed in the SEM (Fig. 3(d) and (e)). Thus the HGMs treated with 2.5 mol/L HF were used for the following treatments.

Fig. 4 shows the XRD patterns of HGMs treated at different steps of (a) pristine SiO_2, (b) roughening by HF, (c) activation by $PdCl_2$ and (d) Ni plating. Although SiO_2 reacted with HF preferably, but the SiF_4 product was in gas state which volatilized soon afterwards [30].

$$SiO_2 + 4HF \rightarrow SiF_4 \uparrow + 2H_2O \quad (5)$$

Therefore, no other phase peaks were identified except SiO_2 after the roughening step by HF. It also can be noticed that the activation step has no effects on the XRD patterns of HGMs because only a trace amount of Pd nanoparticles were deposited. After the plating step, Ni peaks were clearly identified, indicating that metallization was successfully achieved on HGMs by electroless chemical plating reaction [18]. However, as only a bit amount of Ni nanoparticles were located on the surface of HGMs (from Fig. 5), and the crystallinity was not so high from the electroless chemical reaction, the Ni peaks were identified very weak in the XRD patterns.

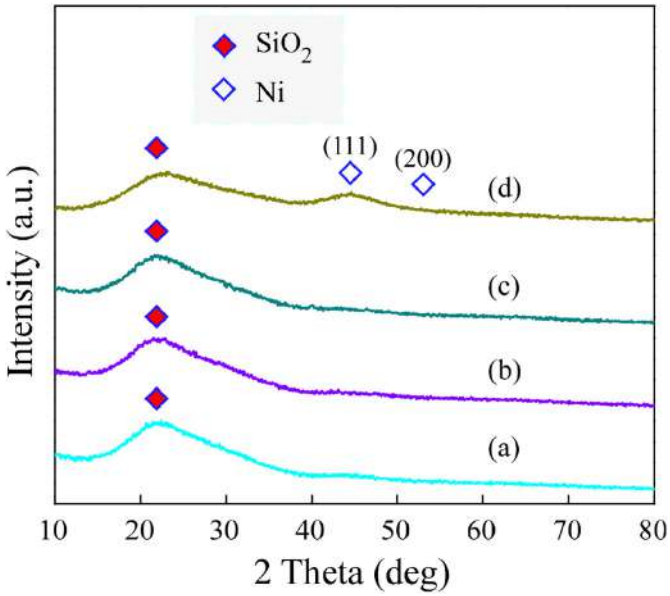

Fig. 4. XRD patterns of SiO_2 treated at different steps of (a) Pristine SiO_2, (b) roughening by HF, (c) activation by $PdCl_2$, (d) Ni plating.

The SEM images of HGMs treated at different steps were shown in Fig. 5, (a) pristine HGMs, (b) roughening by HF, (c) activation by $PdCl_2$, (d) Ni plating. The experimental conditions were kept the same with

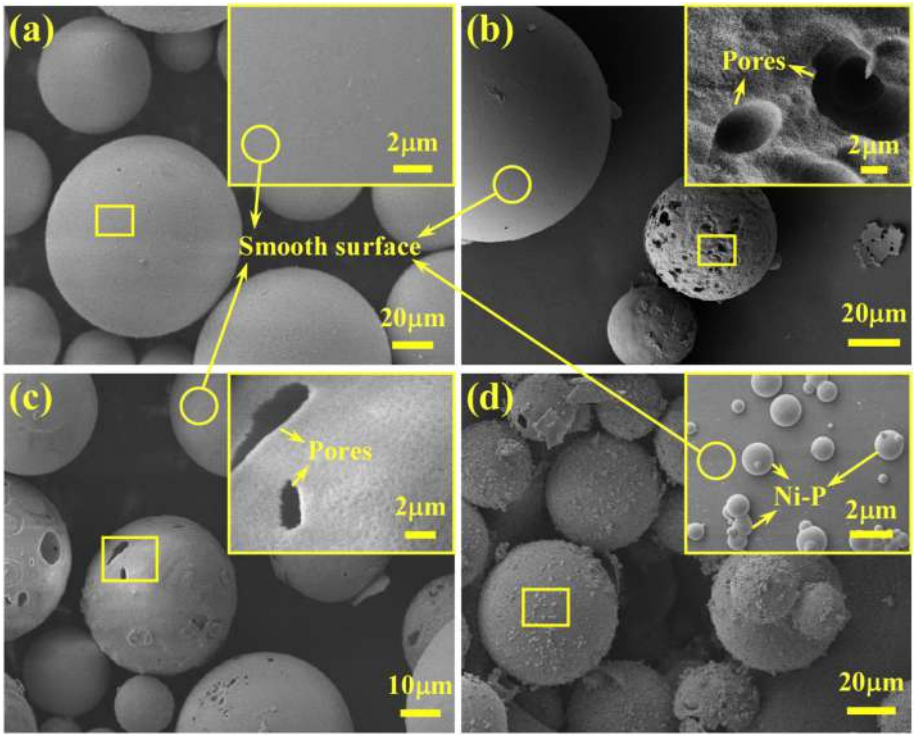

Fig. 5. SEM images of HGMs treated at different steps: (a) pristine HGMs, (b) roughening by HF, (c) activation by $PdCl_2$, (d) Ni plating.

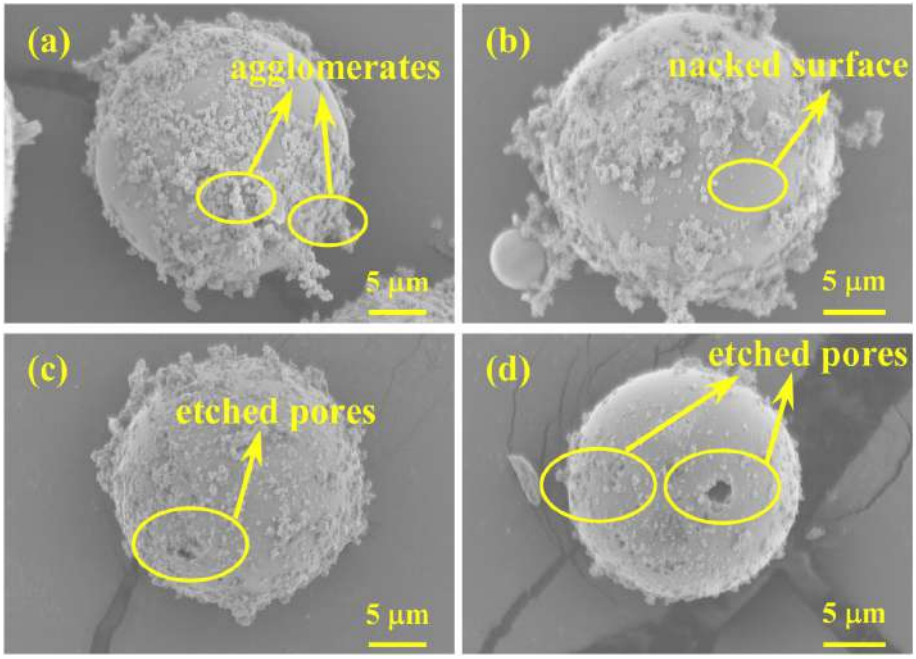

Fig. 6. SEM images of Ni plated HGMs after immersing in 0.1 L $NiSO_4$ solution with the weight of HGMs as (a) 0.5 g, (b) 1 g, (c) 1.5 g, (d) 2 g, HGMs were roughened by HF (2.5 mol/L).

those of Fig. 4. The specific surface area and surface energy of HGMs increased after the surface roughening process, for which the adsorption of the Pd nanoparticles activator to the HGMs was also enhanced. After roughening and activation processes (Fig. 5(b) and (c)), some pores were observed clearly, indicating the excessive roughening of HGMs by HF. Therefore, some agglomeration of plated Ni nanoparticles (Fig. 5(d)) was identified on the surface of HGMs, and some pores still exist there without Ni plating. Furthermore, Fig. 6 shows the SEM images of Ni plated HGMs after immersing in 0.1 L $NiSO_4$ solution with the weight of HGMs as (a) 0.5 g, (b) 1 g, (c) 1.5 g, (d) 2 g. Almost no continuous and uniform Ni nanoparticles were dispersed on the surface of HGMs at a low weight of 0.5 g. With increasing the weight of immersed HGMs to 1 g, 1.5 g and 2 g, the amount of Ni nanoparticles precipitated on the surface of HGMs decreased continuously, but still agglomerated, and some pores were exposed. Due to the uneven roughening by HF, the surface of HGMs with a different roughness could not adsorb enough activated palladium particles after the activation step, and thus could not provide enough nucleation centers

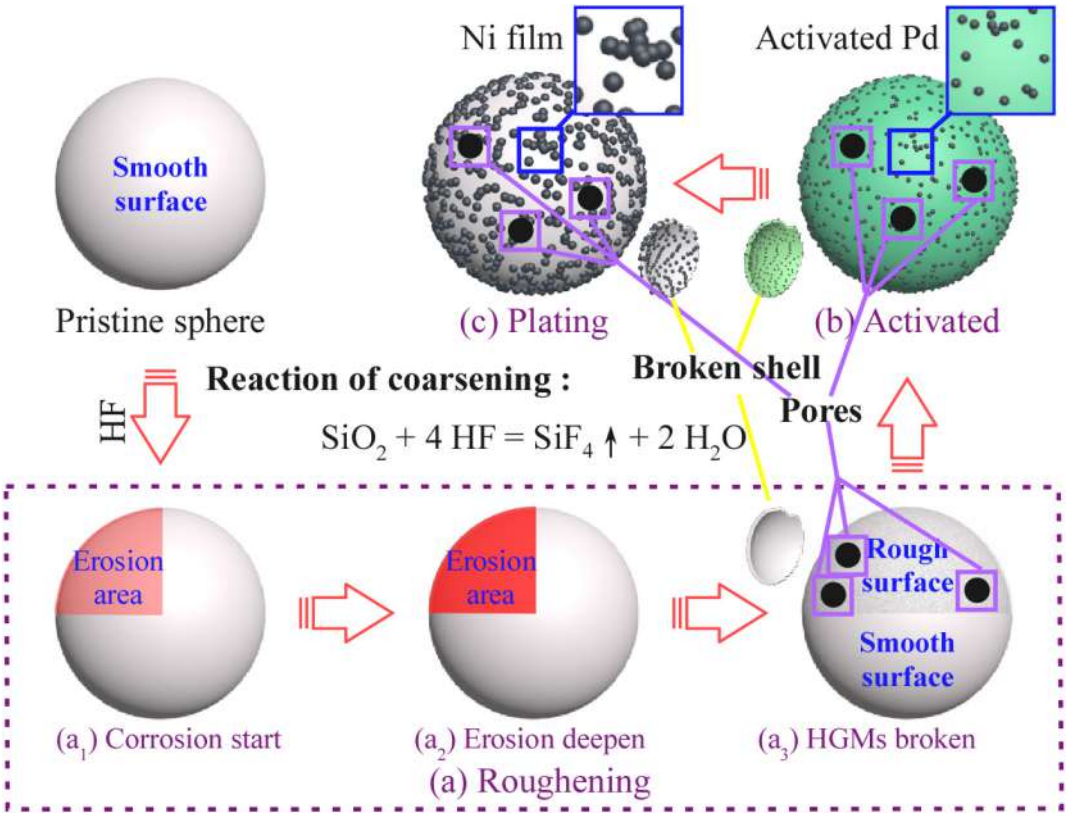

Fig. 7. The schematic of roughening by HF and Ni plating.

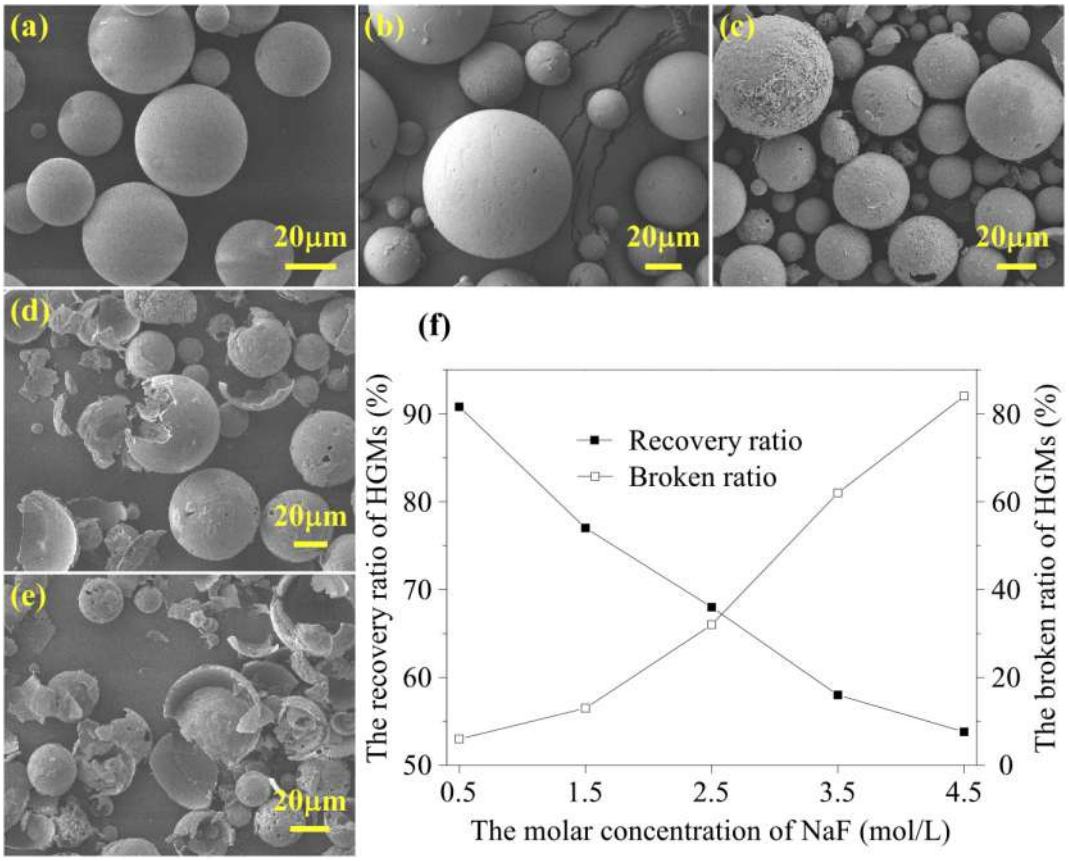

Fig. 8. SEM images of alkaline washed HGMs roughened with different concentrations of NaF and HCl at (a) 0.5 mol/L, (b) 1.5 mol/L, (c) 2.5 mol/L, (d) 3.5 mol/L, (e) 4.5 mol/L and (f) the recovery ratio and broken ratio of HGMs roughened with different concentrations of NaF.

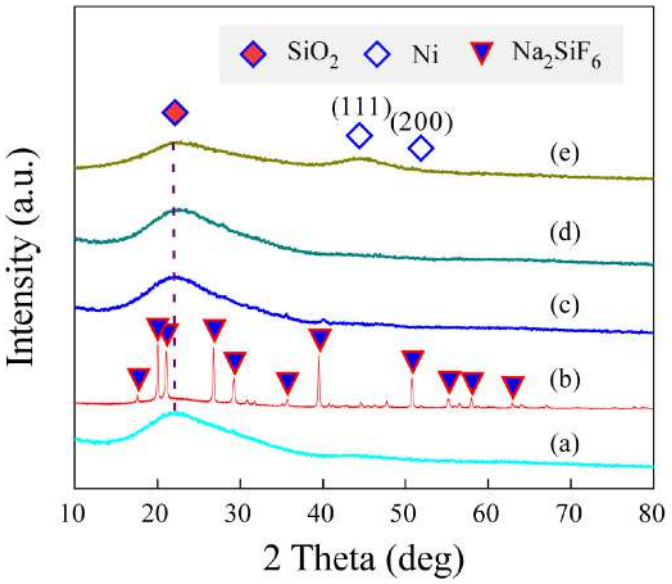

Fig. 9. XRD patterns of SiO_2 treated by different steps of (a) pristine SiO_2, (b) roughening by NaF + HCl, (c) alkaline washing by NaOH, (d) activation by $PdCl_2$, (e) Ni plating.

effectively for even Ni plating.

Based on the above experimental results, Fig. 7 presents the schematic roughening mechanism by HF, together with the followed activation and Ni plating steps. As the reaction of HF with SiO_2 of HGMs happened rapidly, serious damage as shown in Fig. 7 (b1, b2, b3) appeared with holes and even broken fragments. In the activation process, these pores and fragments would absorb more Pd nanoparticles than roughened surface of HGMs. Therefore, the Ni nanoparticles would also be deposited on these pores and fragments preferentially, resulting in the poor uniformity of chemical plating.

3.2. NaF + HCl roughening

Fig. 8 shows the SEM images of HGMs roughened with different concentrations of NaF at (a) 0.5 mol/L, (b) 1.5 mol/L, (c) 2.5 mol/L, (d) 3.5 mol/L, (e) 4.5 mol/L and (f) the dependence of recovery ratio/broken ratio on NaF concentrations. At a low NaF concentration of 0.5 mol/L, the recovery ratio of microspheres is almost 91.3%, and the broken ratio is only about 6%, with a preferred integrity (Fig. 8(a)). With increasing the HF concentration to 2.5 mol/L, although the recovery ratio of the microspheres decreases linearly and the broken ratio increases rapidly, reaching 68.5% and 34.3%, respectively. The further increase of NaF concentration would cause the breakage degree of HGMs was alleviated apparently compared to those treated by HF as shown in Fig. 3.

Fig. 9 shows the XRD patterns of (a) HGMs and those treated by different steps (b) roughening by NaF + HCl, (c) alkaline washing by NaOH, (d) activation by $PdCl_2$, and (e) Ni plating. After roughening by NaF + HCl, the peaks indexed to Na_2SiF_6 (JCPDS 33–1280) were identified as shown in Fig. 9(b), quite different from the results by HF as shown in Fig. 4(b), suggesting that SiO_2 reacted with NaF to form water-insoluble Na_2SiF_6 according to the Eq. (4).

$$SiO_2 + 6NaF + 4HCl \rightarrow Na_2SiF_6 \downarrow + 4NaCl + 2H_2O \quad (6)$$

As shown in Fig. 9(c), however, the peaks of Na_2SiF_6 disappeared after alkali washing due to the reaction (5) of Na_2SiF_6 with NaOH to form water soluble Na_2SiO_3 and NaF [31].

$$Na_2SiF_6 + 6NaOH \rightarrow Na_2SiO_3 + 6NaF + 3H_2O \quad (7)$$

After surface activation and electroless chemical plating, the peaks of Ni-phosphorus alloy appeared in the XRD spectrum of Fig. 9(e), indicating that metallization was successfully achieved on the surface of HGMs. Just like Fig. 4, the Ni peaks were also identified very weak due to the low amount and low crystallinity of Ni nanoparticles.

The appearance and elimination of Na_2SiF_6 after the roughening and alkali washing steps can also be verified from SEM observation in Fig. 10 and EDX mapping in Fig. 11. The specific surface area and surface energy of HGMs both increased after the surface roughening process by HF or NaF, for which the adsorption of the Pd nanoparticles activator to the HGMs was also enhanced. But after NaF roughening, the surface of HGMs was covered by sediments of Na_2SiF_6 according to XRD patterns of Fig. 9 and the corresponding EDX mapping in Fig. 11. Such Na_2SiF_6 by-products reacted with NaOH to from water-dissolvable $NaSiO_3$ and NaF. The surface of HGMs was exposed without any obvious pores or breakage. Such a modified roughening and followed alkali washing method can thus not only avoid uneven surface roughening, but also hinder the further damage of HGMs by covering Na_2SiF_6 sediments. Therefore, Ni was uniformly and successively distributed on

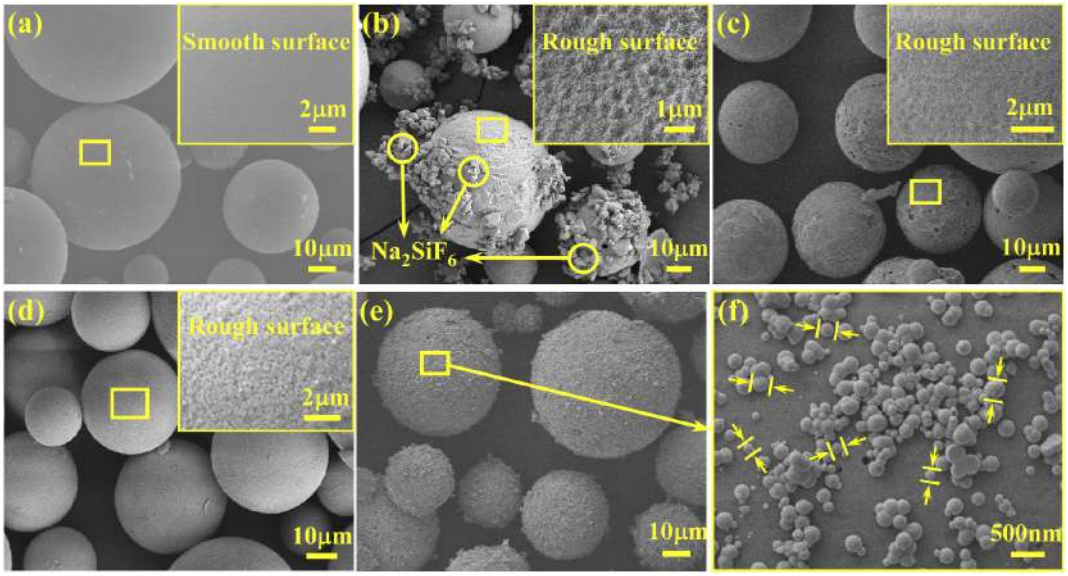

Fig. 10. SEM images of SiO_2 from pretreatment and Ni plating (a) pristine HGMs, (b) roughened by NaF and HCl, (c) alkaline washed by NaOH, (d) activation by $PdCl_2$, (e) Ni plated by $NiSO_4$ solution, (f) high magnification SEM images of (e).

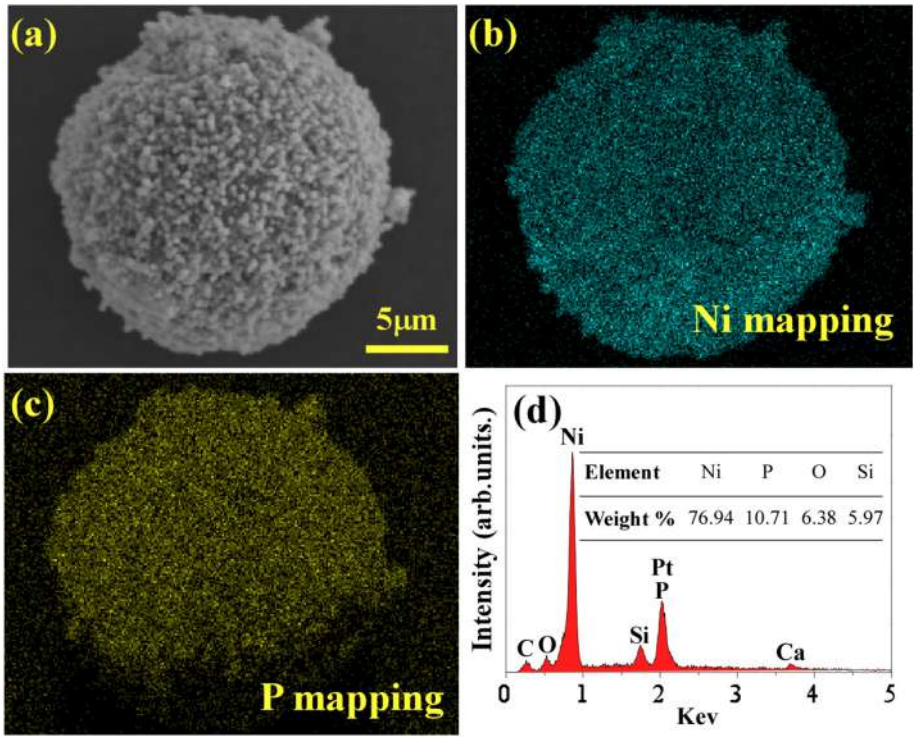

Fig. 11. (a) SEM image of Ni plated HGMs, (b) Ni mapping, (c) P mapping, (d) EDX spectrum.

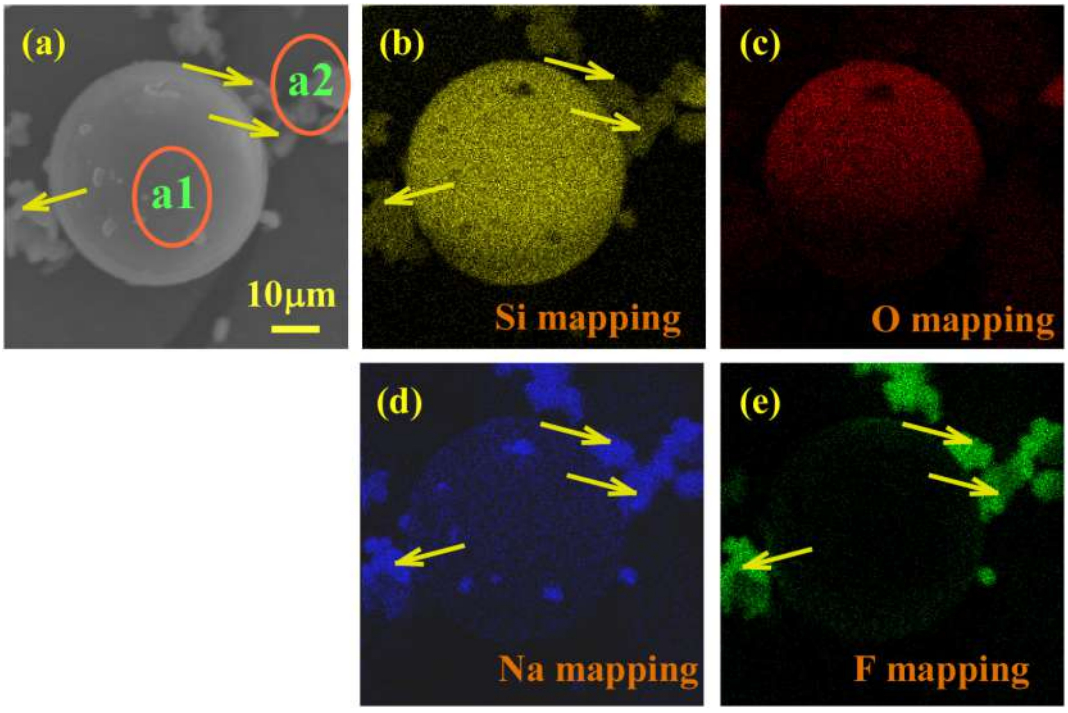

Fig. 12. (a) SEM image of HGMs roughened by NaF + HCl, (b) Si mapping, (c) O mapping, (d) Na mapping, (e) F mapping.

HMGs, which was validated from the SEM images (Fig. 10(d)) and EDX mapping in Fig. 12. Furthermore, Fig. 13 shows the SEM images of Ni plated HGMs after immersing in 0.1 L $NiSO_4$ solution with the weight of HGMs as (a) 0.5 g, (b) 1 g, (c) 1.5 g, (d) 2 g. Ni nanoparticles were found to distribute much more uniformly on the surface of HGM than those in Fig. 6, validating the benefits of the NaF roughening effects. In addition, compared with the commercial product, our Ni-plated HGMs by NaF roughening also have the obvious merits of low cost, low breakage and uniform coverage of the metal nanoparticles on the surface of HGMs.

It should be noticed that the adhesion is an important factor to determine the quality of the coating. Although a very exact value of the adhesion was difficult to obtain due to the small diameter and large specific surface area, the comparison is possible from the Ni-plated images as shown in Fig. 6 and Fig. 11, which were conducted from the HF and NaF roughening, respectively. Fig. 6 shows the Ni nanoparticles were agglomerated and even some random ones were distributed not on

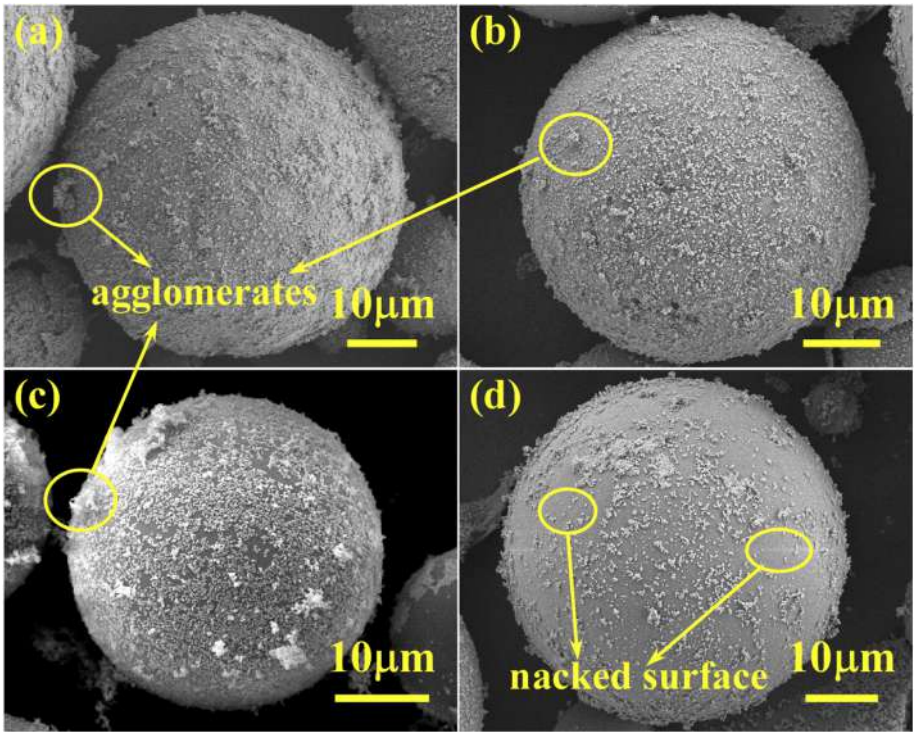

Fig. 13. SEM images of Ni plated HGMs after immersing in 0.1 L $NiSO_4$ solution. The weight of HGMs is (a) 0.5 g, (b) 1 g, (c) 1.5 g, (d) 2 g, HGMs were roughened by NaF (2.5 mol/L).

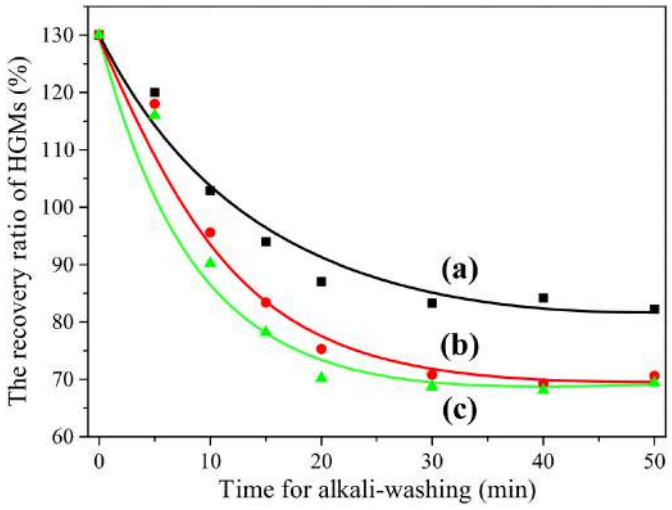

Fig. 14. The recovery ratio of HGMs which roughened with 2.5 mol/L NaF and alkaline washed with different concentrations of NaOH at (a) 20 g/L, (b) 30 g/L, (c) 40 g/L.

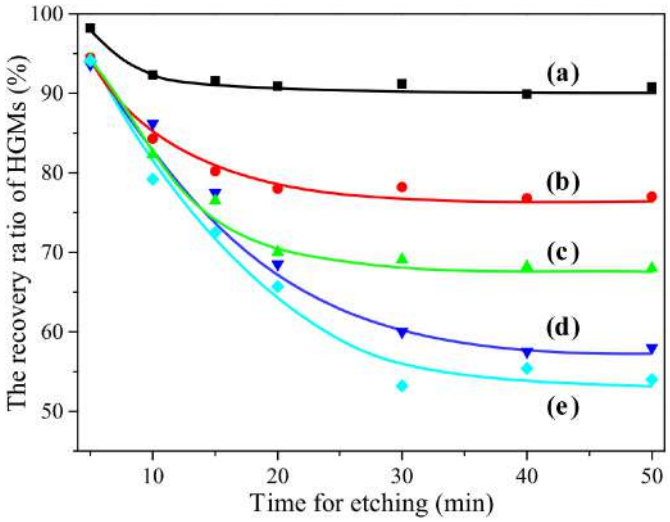

Fig. 15. The recovery ratio of HGMs by roughening with different concentrations of NaF at (a) 0.5 mol/L; (b) 1.5 mol/L, (c) 2.5 mol/L, (d) 3.5 mol/L, (e) 4.5 mol/L.

the surface of HGMs. The distribution of Ni nanoparticles on HGMs was relatively uniform in Fig. 11, also indicating a good adhesion of Ni nanoparticles with HGMs, which could be attributed to the uniform roughening of HGMs by NaF. On the other hand, in order to get a uniform and complete Ni coating, a proper ratio of microspheres to liquid as 1 g/0.1 L was obtained in the presents study. Simultaneously, the thickness of the coating was measured to be 160–250 nm, on the assumption of spherical Ni nanoparticles.

Fig. 14 shows the effect of NaOH concentration on the recovery ratio of HGMs after NaOH washing of roughened HGMs by NaF at 2.5 mol/L. At a high concentration of NaOH of 30 and 40 g/L, the alkali-washing time became much shorter and recovery ratio were almost the same as about 70%, suggesting Na_2SiF_6 could be dissolved completely in the NaOH solution. On the other hand, Fig. 15 shows the recovery ratio after NaOH washing of roughened HGMs by NaF at 0.5 to 4.5 mol/L. Overall, the curves were observed to drop and become flat soon, indicating the roughening reaction end time has a strong dependence on the concentration of NaF. About 77% of the HGMs was recovered after NaOH washing in the NaF solution of 1.5 mol/L. But the recovery ratio decreased to 53.8% after NaOH washing of roughened HGMs by NaF of 4.5 mol/L, because more Na_2SiF_6 formed from the reaction of SiO_2 with NaF were washed away by NaOH.

In order to further study the erosion behavior by acid roughening, the proportion of NaF contributed to the generation SiF_4 and Na_2SiF_6 was tested as shown in Fig. 16. It is clearly observed that 16% NaF contributed to the formation of Na_2SiF_6 when the concentration of NaF

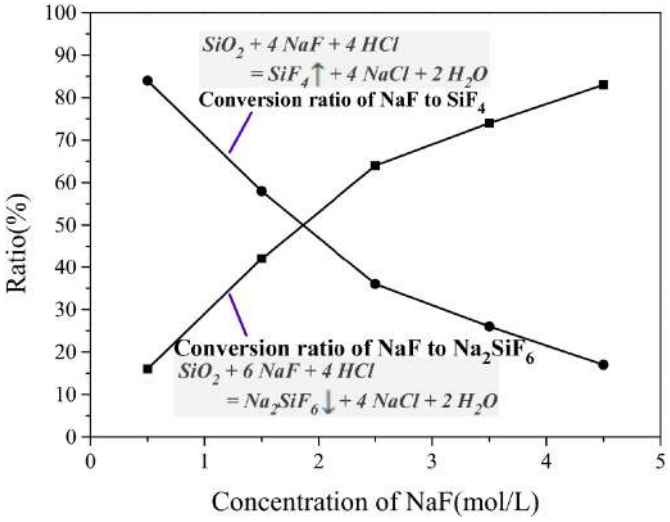

Fig. 16. The ratio of NaF used to generate SiF_4 or Na_2SiF_6 at different concentrations of NaF.

is as low as 0.5 mol/L, suggesting that the process of acid roughening is basically similar with that by HF at 0.5 mol/L, with the only difference of slower corrosion rate. With increasing the concentration of NaF to 2.5 and 4.5 mol/L, however, a much higher proportion NaF, 64% and 83%, contributed to the formation of Na_2SiF_6, respectively. On the one hand, it should be noticed that although uniform corrosion, the degree of corrosion will deepen to make the shell of microspheres thinner and easy breakage, which has been validated in the SEM observation of Fig. 8(c) and (d).

Based on the above experimental results and analysis, a schematic mechanism is given for the present modified roughening and electroless chemical plating, as shown in Fig. 17. Firstly, NaF dissolves in HCl solution to release F ion to corrode HGMs by the reaction of NaF with SiO_2 to form Na_2SiF_6, which would simultaneously cover the corroded surface of HGMs to hinder further damage. Therefore, at an appropriate NaF concentration, the corrosion reaction would like to cause the uniform roughening of HGMs as anticipated. The following NaOH washing and the common Pd activation, would provide more uniform active sites for the uniform and fine Ni plating as well. However, the excessive NaF would also cause the serious damage of the HGMs just as verified in Fig. 8 of this study, suggesting that experimental optimization is still necessary to get uniform and perfect electroless chemical plating on HGMs.

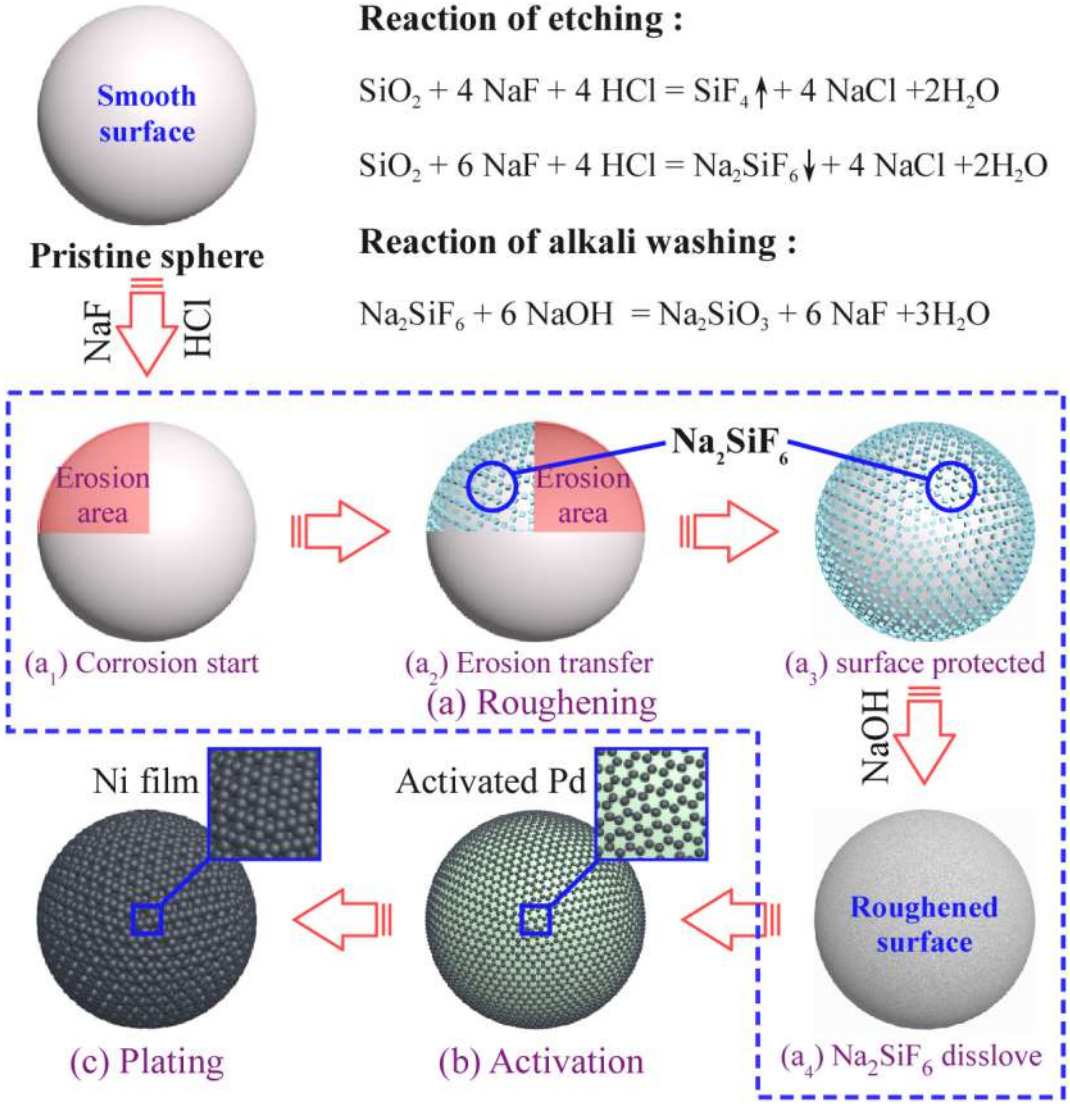

Fig. 17. The schematic of roughening by NaF + HCl and Ni plating.

4. Conclusions

A new NaF roughening and NaOH washing strategy instead of HF was successfully applied in the present study to alleviate the damage and breakage of HGMs. The XRD and SEM analysis indicated that NaF roughened HGMs by reacting with SiO_2 to form Na_2SiF_6, which covered the surface and protected HGMs from uneven roughening. However, a high NaF concentration would also cause the serious damage of the HGMs, suggesting that experimental optimization is still necessary. The following NaOH washing was also found vital for uniform Ni plating and recovery of the HGMs as well. After electroless plating, Ni nanoparticles as a shell were found to distribute much more uniformly and tightly on the surface of HGM roughened by NaF than HF.

Acknowledgements

The authors would like to acknowledge the financial supports from Fundamental Research Funds for the Central Universities (2015B01914), National Natural Science Foundation of China (50979028, 51502092), Natural Science Foundation of Jiangsu Province (BK20161506) and National 973 Plan Project (2015CB057803).

References

[1] C.D. Mcauliffe, Oil-in-water emulsions and their flow properties in porous media, J. Pet. Technol. 25 (1973) 727–733.
[2] Y. Guo, Z. Cao, D. Wang, S. Liu, Improving the friction and abrasion properties of nitrile rubber hybrid with hollow glass beads, Tribol. Int. 101 (2016) 122–130.
[3] M. Palumbo, G. Donzella, E. Tempesti, P. Ferruti, On the compressive elasticity of epoxy resins filled with hollow glass microspheres, J. Appl. Polym. Sci. 60 (1996) 47–53.
[4] M.L. Schmitt, J.E. Shelby, M.M. Hall, Preparation of hollow glass microspheres from sol–gel derived glass for application in hydrogen gas storage, J. Non-Cryst. Solids 352 (2006) 626–631.
[5] S.K. Jain, G.P. Agrawal, N.K. Jain, A novel calcium silicate based microspheres of repaglinide: in vivo investigations, J. Control. Release Soc. 113 (2006) 111–116.
[6] R. Zhou, H. Chen, G. Liu, G. Zhao, Y. Liu, Conductive and magnetic glass microsphere/cobalt composites prepared via an electroless plating route, Mater. Lett. 112 (2013) 97–100.
[7] S.T. Kim, S.S. Kim, Electroless plating of Co thin film on hollow glass microspheres and the effect of film thickness on microwave absorbance, IEEE Trans. Magn. 48 (2012) 3494–3497.
[8] S. Zhou, Q. Zhang, L. Hao, G. Xuan, H. Jin, Microwave absorption performance of magnetic Fe–Ni–P nanoparticles electrolessly plated on hollow glass microspheres, Mater. Chem. Phys. 134 (2012) 224–228.
[9] J. Pang, Q. Li, W. Wang, X. Xu, J. Zhai, Preparation and characterization of electroless Ni–Co–P ternary alloy on fly ash cenospheres, Surf. Coat. Technol. 205 (2011) 4237–4242.
[10] Z. An, J. Zhang, S. Pan, Fabrication of glass/Ni-Fe-P ternary alloy core/shell composite hollow microspheres through a modified electroless plating process, Appl. Surf. Sci. 255 (2008) 2219–2224.
[11] J. Pang, Q. Li, B. Wang, D. Tao, X. Xu, W. Wang, J. Zhai, Preparation and characterization of electroless Ni-Fe-P alloy films on fly ash cenospheres, Powder Technol. 226 (2012) 246–252.
[12] S.S. Kim, S.T. Kim, J.M. Ahn, K.H. Kim, Magnetic and microwave absorbing properties of Co–Fe thin films plated on hollow ceramic microspheres of low density, J. Magn. Magn. Mater. 271 (2004) 39–45.
[13] G.S. Czok, J. Werther, Liquid spray vs. gaseous precursor injection — its influence on the performance of particle coating by CVD in the fluidized bed, Powder Technol. 162 (2006) 100–110.
[14] M. Karches, P.R.V. Rohr, Microwave plasma characteristics of a circulating fluidized bed-plasma reactor for coating of powders, Surf. Coat. Technol. 142 (2001) 28–33.
[15] M.P. Singh, H. Singh, O. Singh, N. Kohli, R.C. Singh, Preparation and characterization of nanocrystalline WO powder based highly sensitive acetone sensor, Indian J. Phys. 86 (2012) 357–361.
[16] X. Yu, Z. Shen, Z. Xu, Preparation and characterization of Ag-coated cenospheres by magnetron sputtering method, Nucl. Inst. Methods Phys. Res. A 265 (2007) 637–640.
[17] S. Shukla, S. Seal, J. Akesson, R. Oder, R. Carter, Z. Rahman, Study of mechanism of electroless copper coating of fly-ash cenosphere particles, Appl. Surf. Sci. 181 (2001) 35–50.
[18] Q. Zhang, M. Wu, W. Zhao, Electroless nickel plating on hollow glass microspheres, Surf. Coat. Technol. 192 (2005) 213–219.
[19] A. Zeng, W. Xiong, X. Jian, Electroless Ni-P coating of cenospheres using silver nitrate activator, Surf. Coat. Technol. 197 (2005) 142–147.
[20] S. Shukla, S. Seal, Z. Rahaman, K. Scammon, Electroless copper coating of cenospheres using silver nitrate activator, Mater. Lett. 57 (2002) 151–156.
[21] X.F. Meng, D.H. Li, X.Q. Shen, W. Liu, Preparation and magnetic properties of nano-Ni coated cenosphere composites, Appl. Surf. Sci. 256 (2010) 3753–3756.
[22] H. Zhang, Z.X. Kang, J. Sang, H. Hirahara, Surface metallization of ABS plastics for nickel plating by molecules grafted method, Surf. Coat. Technol. 340 (2018) 8–16.
[23] H.J. Hu, Z. Cao, X.G. Liu, X.G. Feng, Y.G. Zheng, K.F. Zhang, H. Zhou, Effects of substrate roughness on the vacuum tribological properties of duplex PEO/bonded-MoS2 coatings on Ti6Al4V, Surf. Coat. Technol. 349 (2018) 593–601.
[24] X. Zheng, J. Tan, Q. Zhang, M. Wang, L. Meng, Effect of laser surface texturing depth on the adhesion of electroless plated nickel coating on alumina, Surf. Coat. Technol. 311 (2017) 151–156.
[25] X.G. Cao, H.Y. Zhang, Study of pretreatment techniques and characterization of electroless silver on cenospheres, Electron. Mater. Lett. 8 (2012) 519–522.
[26] A. Kaewvilai, R. Tanathakorn, A. Laobuthee, Electroless copper plating on nano-silver activated glass substrate: a single-step activation, Surf. Coat. Technol. 319 (2017) 260–266.
[27] W.-J. Kim, S.-S. Kim, Preparation of Ag-coated hollow microspheres via electroless plating for application in lightweight microwave absorbers, Appl. Surf. Sci. 329 (2015) 219–222.
[28] V. Genova, L. Paglia, F. Marra, C. Bartuli, G. Pulci, Pure thick nickel coating obtained by electroless plating: surface characterization and wetting properties, Surf. Coat. Technol. 357 (2019) 595–603.
[30] W.U. Bo wan, J.N. Liu, New principle and phenomena of experiment on hydrofluoric acid's corroding glass, J. Shaanxi Normal Univ. 30 (2002) 147–148.
[31] Y. Zong, A.J. Tang, Q.Y. Wang, M.H. Zhang, S.C. Dou, D.J. Wei, Research of the process for sodium fluosilicate prepared from SiF_4, Guangzhou Chem. Ind. 41 (2013) 82–84.